

Effective Exchange Interactions for Bad Metals and Implications for Iron-based Superconductors

Wenxin Ding^{1,2,*}, Rong Yu³, Qimiao Si², and Elihu Abrahams^{4†}

¹*School of Physics and Material Science, Anhui University, Hefei, 230601, China*

²*Department of Physics & Astronomy, Rice University, Houston, Texas 77005, USA*

³*Physics Department and Beijing Key Laboratory of Opto-electronic Functional Materials and Micro-nano Devices, Renmin University, Beijing 100872, China*

⁴*Department of Physics and Astronomy, University of California Los Angeles, Los Angeles, California 90095, USA*

(Dated: March 3, 2022)

The experimentally observed bad metal behavior in parent iron pnictides and chalcogenides suggests that these systems contain strong electronic correlations and are on the verge of a metal-to-insulator transition. The magnetic excitations in this bad-metal regime mainly derive from the incoherent part of the electronic spectrum away from the Fermi energy. We present a microscopic study of the exchange interactions in such a regime within a slave rotor approach. We find that the exchange interaction is maximized near the Mott transition. Generalizations to the multi-orbital case are discussed, as are the implications for the strength of superconducting pairing amplitude in iron-based superconductors.

Introduction: Superconductivity in the iron pnictides and chalcogenides occurs at the border of antiferromagnetic order [1, 2]. For an understanding of the superconductivity, it is important to characterize the magnetism. An important clue for the latter is that the parent iron pnictides are bad metals. Their electrical resistivity at room temperature is very large, reaching the Mott-Ioffe-Regel limit ($k_F \ell < 2\pi$) [3, 4]. Optical conductivity measurements show a large suppression of the Drude weight [5], which suggests that the majority of the electronic excitations lives in the incoherent part away from the Fermi energy and the system is in proximity to a Mott insulator [6–8]. The role of the correlation effects is further highlighted by the observation of both the insulating states [9–13] and an orbital-selective Mott phase [14, 15] in a number of iron chalcogenides and it has also been emphasized from a variety of perspectives [16, 17, 19–29].

When the majority of the single-particle excitations are incoherent, they give rise to quasi-localized moments, which are coupled with each other through frustrating exchange interactions [6, 18–21]. This provides a natural basis to understand the large spin spectral weight observed in both the iron pnictides [30] and iron chalcogenides [31–34].

In this paper, we study the exchange interactions in the bad-metal regime. While it is standard to derive superexchange interactions in the Mott localized regime, the microscopic basis for the exchange interactions in the regime of bad metals is much less understood. Here we show how such exchange interactions can be derived in a microscopic framework, using the slave-rotor approach [35, 36]. Important for our analysis is that this approach already contains incoherent excitation spectra at the saddle-point level. We show how such incoherent spectra can be integrated out to yield an exchange interaction, not only for the localized side but also in the bad-metal regime. As a consequence, we show that the exchange interaction is maximized near the Mott transition.

Slave-Rotor Approach: We consider the Hubbard model on a square lattice with only nearest-neighbor hopping

$$H_{HM}(d) = \sum_i H_{at}(i) - \sum_{ij,\alpha} (t_{ij} d_{i\alpha}^\dagger d_{j\alpha} + h.c.), \quad (1)$$

in which $H_{at}(i) = \frac{U}{2} \left(\sum_\alpha d_{i\alpha}^\dagger d_{i\alpha} - N/2 \right)^2$, α is the spin/orbital index running from $\alpha = 1, \dots, N$, with $N=2$ for the one-band model. For definiteness, we will consider a square lattice, and only hopping between nearest-neighbor sites, $\langle ij \rangle$. It is realized that the full energy spectrum of $H_{at}(i)$ can be economically represented by a rotor kinetic energy $H_{at}(i) \rightarrow U \hat{L}_i^2/2$ [35, 36] with $\hat{L}_i = -i\partial_{\theta_i}$, thus providing a tractable reference point for perturbative expansion in t/U . Then in this slave-rotor representation, the bare electron operator is written as a product of the auxiliary rotor fields and a fermionic spinon operator $d_{i\alpha} \equiv f_{i\alpha} e^{-i\theta_i}$, with the constraint $\hat{L}_i = \sum_\alpha (f_{i\alpha}^\dagger f_{i\alpha} - 1/2)$. In place of the phase field one could work with the complex field $e^{i\theta_i} = X_i$, with the additional constraint $|X_i|^2 = 1$. The two constraints are enforced by introducing two Lagrangian multipliers, h_i and λ_i . In terms of the fermionic f_i and complex rotor X_i operators, the physical d_i -electron operator at site i is expressed as follows:

$$d_{i\alpha} \equiv f_{i\alpha} X_i^*. \quad (2)$$

A saddle point arises when one generalizes each X_i to M species so that its symmetry becomes $O(2M)$, scales the hopping t_{ij} to $1/M$, and take the large (N,M) limit with a fixed ratio M/N . In our analysis below, we will write our equations for $N = 2M = 2$.

Using $\partial_\tau \theta_i = -i X_i^* \partial_\tau X_i$, we have the Lagrangian

$$\begin{aligned} \mathcal{L}_{HM} = & \sum_{i,\alpha} f_{i\alpha}^\dagger (\partial_\tau + h_i) f_{i\alpha} + \sum_i \left(\frac{|\partial_\tau X_i|^2}{U} \right. \\ & + \frac{h_i}{U} (X_i^* \partial_\tau X_i - h.c.) + \lambda_i (|X_i|^2 - 1) \Big) \\ & + \sum_{ij,\alpha} (t_{ij} f_{i,\alpha}^\dagger f_{j,\alpha} X_i X_j^* + h.c.). \end{aligned} \quad (3)$$

Note that $\frac{U}{2} \sum_i \hat{L}_i^2 = \frac{|\partial_\tau X_i|^2}{2U}$; we have rescaled U to $U/2$ in Eq. (3) to preserve the correct atomic limit [35].

The saddle point [36, 37] corresponds to decoupling the

spinon-boson coupling term via

$$Q_{f,ij} = \langle X_j^* X_i \rangle, \quad Q_{X,ij} = \langle \sum_\alpha f_{j\alpha}^\dagger f_{i\alpha} \rangle, \quad (4)$$

which can be formally done by a Hubbard-Stratonovich transformation. These are the channels that preserve physical fermion numbers. The Lagrangian \mathcal{L}_{HM} is decoupled into two parts:

$$\mathcal{L}_{MF,f} = \sum_{i,\alpha} f_{i\alpha}^\dagger (\partial_\tau + h_i) f_{i\alpha} + t \sum_{\langle ij \rangle, \alpha} (Q_f f_{i\alpha}^\dagger f_{j\alpha} + h.c.), \quad (5)$$

$$\begin{aligned} \mathcal{L}_{MF,X} = & \sum_i \left(\frac{|\partial_\tau X_i|^2}{U} + \frac{h}{U} (X_i^* \partial_\tau X_i - h.c.) \right. \\ & \left. + \lambda_i |X_i|^2 \right) + t \sum_{\langle ij \rangle} (Q_X X_i X_j^* + h.c.). \end{aligned} \quad (6)$$

The diagrams shown in Fig. 1(a) correspond to the saddle point (see below). From here on, we drop the ij index for t , keeping only the nearest neighbor hopping, and also that for $Q_{f(X)}$, assuming translational invariance throughout this paper. Then the spinon and X -field Green's functions at the saddle-point level read

$$G_f(\omega; \mathbf{k}) = (i\omega + h - Q_f \epsilon_{\mathbf{k}})^{-1}, \quad (7)$$

$$G_X(\nu; \mathbf{k}) = (\nu^2/U + 2ih\nu/U + \lambda + Q_X \epsilon_{\mathbf{k}})^{-1}, \quad (8)$$

where $\epsilon_{\mathbf{k}} = -2t[\cos(k_x) + \cos(k_y)]$ is the bare lattice dispersion function. For the saddle point solution, the Lagrangian multipliers become uniform: $h_i \rightarrow h$ and $\lambda_i \rightarrow \lambda$. The self-consistent equation which determines λ reads

$$\int \frac{d^2 k}{(2\pi)^2} \sum_\nu G_X(\nu; \mathbf{k}) = 1. \quad (9)$$

The h is determined by $\langle \hat{L} \rangle = \sum_\alpha (\langle f_{i\alpha}^\dagger f_{i\alpha} \rangle - 1/2)$. For the half-filling case we consider, $h = 0$ for arbitrary U .

In both the insulating phase and the metallic phase, the spinons are always treated as free fermions at half-filling. We find $Q_X = \langle \sum_\alpha f_{i\alpha}^\dagger f_{j\alpha} \rangle = 8/\pi^2$, irrespective of U . Thus self-consistency is automatically satisfied. Q_f in general decays with increasing U , and in the large- U limit $Q_f \simeq 2/U$. The Mott transition is realized when U reaches U_c where $(\lambda + Q_X \epsilon_{\mathbf{k}=0})$ vanishes, so the X -field starts to condense. For $U < U_c$, we can divide the rotor field into a condensate and an incoherent component: $X_i \rightarrow X_i^0 + X_i'$ and, correspondingly, the X -field Green's function can be written as

$$G_X(\nu; \mathbf{k}) = Z \delta(\nu) \delta(\mathbf{k}) + G_{X,\text{inc}}, \quad (10)$$

where $G_{X,\text{inc}} = \langle X_{\mathbf{k}}'^* X_{\mathbf{k}}' \rangle = (\nu^2/U + \lambda_C + Q_X \epsilon_{\mathbf{k}})^{-1}$ and $Z = (X_i^0)^2$. In the metallic phase, $\lambda = \lambda_C$ remains a constant, determined by $\lambda_C = -Q_X \epsilon_{\mathbf{k}=0}$. Then from Eq. (9), we find

$$Z = 1 - \sqrt{U/U_c}, \quad (11)$$

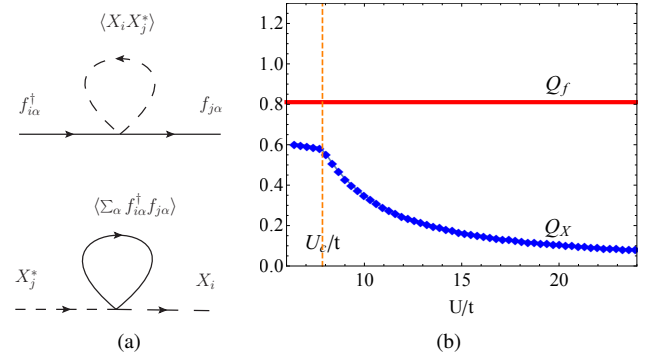


FIG. 1. (a) Feynman diagrams corresponding to the saddle point equations. (b) The self-consistent parameters Q_f and Q_X plotted as function of U/t .

with U_c is determined from $\int \frac{d\nu d^2 k}{(2\pi)^3} (\nu^2/U_c + \lambda_C + Q_X \epsilon_{\mathbf{k}})^{-1} = 1$. The spinon Green's function Eq. (7) remains the same (up to the renormalization factor Q_f). The division of the d -electron excitations into coherent and incoherent parts is thus realized by separating the rotor field X into a condensate and a fluctuating part. The parameters Q_f and Q_X computed numerically as a function of U/t are shown in Fig. 1(b).

Exchange Interaction from Integrating Out Incoherent Excitations: Beyond the saddle point, the spinon and rotor fields are coupled. To introduce these couplings, we consider Eq. (3) diagrammatically. \mathcal{L}_{HM} contains various bare interaction vortices as shown in Fig. 2(a). The most important one is the first, a spinon-rotor vortex; it corresponds to the hopping of the physical electrons. The others come from the constraints being enforced by the Lagrangian multiplier fields.

We first (formally) integrate out either the spinons ($f_{i\alpha}$ s) or the rotors (X_i s) from the full \mathcal{L}_{HM} of Eq. (3) to obtain effective actions $S^{\text{eff},X}(X_i)$ or $S^{\text{eff},f}(f_{i\alpha})$:

$$\begin{aligned} S^{\text{eff},f} &= S^{0,f} - \ln \det \left[\begin{pmatrix} (G_X^0)^{-1} & t \sum f_{i\alpha}^\dagger f_{j\alpha} \\ t \sum f_{j\alpha}^\dagger f_{i\alpha} & (G_f^0)^{-1} \end{pmatrix}_{i,j} \right], \\ S^{\text{eff},X} &= S^{0,X} - \ln \det \left[\begin{pmatrix} (G_f^0)^{-1} & t X_i^* X_j \\ t X_j^* X_i & (G_X^0)^{-1} \end{pmatrix}_{i,j} \right], \end{aligned} \quad (12)$$

where

$$\begin{aligned} S^{0,f} &= \int d\tau \mathcal{L}^{0,f} = \int d\tau \sum_{i,\alpha} f_{i\alpha}^\dagger \partial_\tau f_{i\alpha}, \\ S^{0,X} &= \int d\tau \mathcal{L}^{0,X} = \int d\tau \sum_i \left(\frac{|\partial_\tau X_i|^2}{U} + \lambda |X_i|^2 \right), \end{aligned}$$

The $\ln \det[\dots]$ can be expanded in orders of t to generate effective hoppings and interactions. We take a renormalized expansion, so G_f^0 and G_X^0 are replaced by G_f and G_X . To the lowest order in t , we only have the Feynman diagrams shown in Fig. 1(a), which give rise to the saddle point where

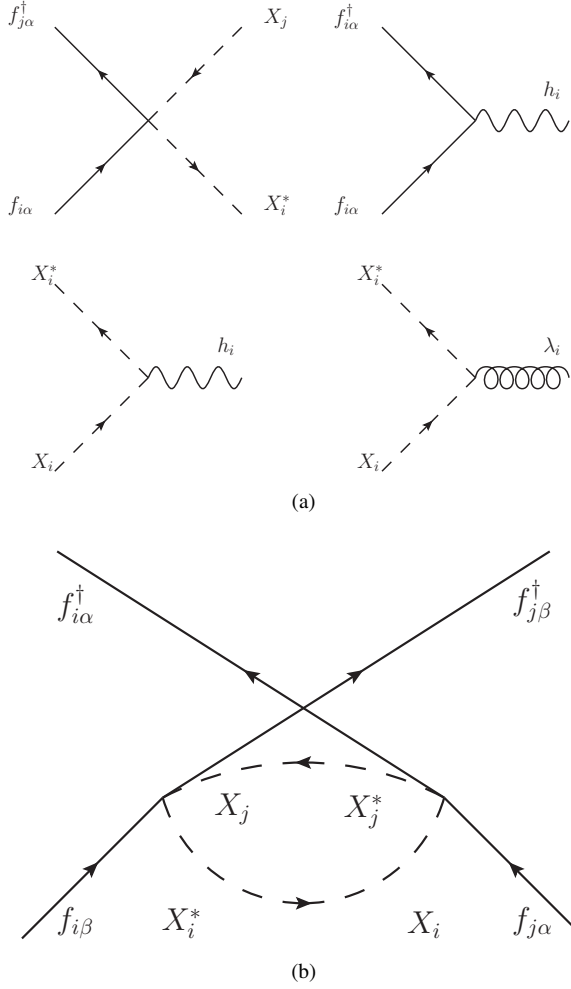


FIG. 2. (Color online) (a) Bare interaction vortices. (b) Feynman diagram for the effective spin exchange interaction.

G_f and G_X are computed self-consistently. Again, for the metallic phase, we need to decompose the rotor fields into a condensate component and a fluctuating component: $X_i \rightarrow X_i' + X_i^0$.

For $S^{\text{eff},f}$ at $\mathcal{O}(t^2)$, we have the exchange vortex shown in Fig. (2(b)). This diagram yields a magnetic exchange interaction,

$$\begin{aligned} H_{f;\text{ex}} &= \frac{J_{\text{ex}}}{2} \sum_{\langle ij \rangle} \sum_{\alpha, \beta} f_{i\alpha}^\dagger f_{i\beta} f_{j\beta}^\dagger f_{j\alpha} \\ &= J_{\text{ex}} \sum_{\langle ij \rangle} \mathbf{S}_i \cdot \mathbf{S}_j, \end{aligned} \quad (13)$$

where $\mathbf{S}_i = (1/2) \sum_{\alpha, \beta} f_{i\alpha}^\dagger \boldsymbol{\sigma}_{\alpha\beta} f_{i\beta}$ and the factor 1/2 is because it is the second order term of the cumulant expansion. (We have ignored an additive constant in the last equality.)

The exchange interaction is determined by the rotor bubble,

$$J_{\text{ex}} = \int \frac{d\nu}{2\pi} G_X(\nu; i, i) G_X(\nu; j, j), \quad (14)$$

where $G_X(\nu; i, i) = \int \frac{d^2 k}{(2\pi)^2} G_X(\nu; \mathbf{k})$. Note that, this exchange interaction operates in the spin sector, whose energies are low compared to the energies of the incoherent poles of the slave rotors (see below). This makes the equal-time exchange interaction to be essentially the same as the static exchange interaction, for which Eq. (13) describes.

For the latter reference, we contrast the above with a bare perturbative expansion. The latter is based on the following bare atomic actions and bare Green's functions of the spinons and rotors:

$$\begin{aligned} G_X^0(\nu; i, j) &= \delta_{ij} (\nu^2/U + \lambda)^{-1}, \\ G_f^0(\omega; i, j) &= \delta_{ij} (i\omega)^{-1}. \end{aligned} \quad (15)$$

In this procedure, we can also determine an exchange interaction, $J_{\text{ex}}^{\text{bare}}$, from Eq. (14) with G_X replaced by G_X^0 .

Relation to Physical Observables: In the slave rotor representation, the electronic Green's function is calculated via the rotor and spinon Green's functions according to

$$\begin{aligned} iG_d(\omega; \mathbf{k}) &= \\ &- \int d\omega' d\mathbf{k}' G_f(\omega - \omega'; \mathbf{k} - \mathbf{k}') G_X(\omega'; \mathbf{k}'). \end{aligned} \quad (16)$$

This is the Fourier transform of $iG_d(t; \mathbf{x}, \mathbf{x}') = -G_f(t; \mathbf{x}, \mathbf{x}') G_X(-t; \mathbf{x}, \mathbf{x}')$ which stems directly from Eq. (2). In the Mott insulating phase, $G_d(\omega; \mathbf{k})$ is fully gapped due to the large gap from $G_X(\omega; \mathbf{k})$. In the bad metal regime, a coherent quasiparticle part emerges, $G_{d,\text{coh}}(\omega; \mathbf{k}) = Z G_f(\omega; \mathbf{k})$, while the incoherent part still follows from Eq. (16) with $G_X(\omega'; \mathbf{k}')$ replaced by $G_{X,\text{inc}}(\omega'; \mathbf{k}')$.

For the spin operators, because of the constraint in the slave-rotor representation, \mathbf{S}_i (and likewise \mathbf{S}_j) is the same as the physical d -electron spin operator:

$$\mathbf{S}_i = (1/2) \sum_{\alpha, \beta} d_{i\alpha}^\dagger \boldsymbol{\sigma}_{\alpha\beta} d_{i\beta}. \quad (17)$$

Exchange Interaction on the Insulating Side: When U is significantly larger than U_c , the rotor spectrum has a large gap around $\omega = 0$, and two peaks around $\pm U \mathcal{O}(1)$ respectively. The latter characterizes incoherent electronic excitations, which are responsible for $J_{\text{ex}} \sim 1/U$ behavior. Numerical results for large U 's are shown in the inset of Fig. (4), where we also plot the ratio $J_{\text{ex}}/(\gamma t^2/U)$ as a function of U in which γ is determined by $J_{\text{ex}}/(\gamma t^2/U)|_{U \rightarrow \infty} = 1$ to compare with the standard super-exchange interaction. Here we do find $\gamma = 4$, in agreement with the standard result. Note that, the behavior at large U can be qualitatively seen by computing the rotor bubble function with the bare Green's function of the rotors: $J_{\text{ex}}^{\text{bare}}(U \rightarrow \infty) = \int \frac{d\nu}{2\pi} G_X^0(i\nu; i, i) G_X^0(i\nu; j, j)$. Using $\lambda_{U \rightarrow \infty} = U/4$ determined from Eq. (9), we find $J_{\text{ex}}^{\text{bare}} = \frac{\gamma t^2}{U}$. Though $\gamma = 2$ (as opposed to 4 above), $J_{\text{ex}}^{\text{bare}}$ does capture the t^2/U dependence.

Exchange Interaction in the Bad Metal Regime and across the Metal-Insulator Transition: When U approaches U_c

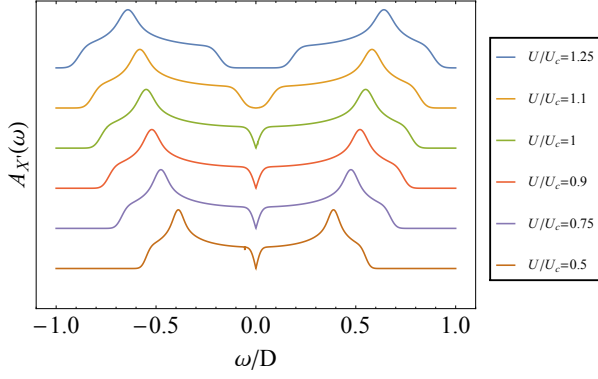


FIG. 3. (Color online) The incoherent spectral function of the slave rotor field plotted versus ω/D for $U/U_c = 1.25, 1.1, 1, 0.9, 0.75, 0.5$ respectively. Here, D is the electron bandwidth $D = 8t$, and each curve is shifted by a different constant. When U is larger than U_c , the rotor spectral weight has a gap around $\omega = 0$. In addition, it has two peaks near $\pm U\mathcal{O}(1)$, which correspond to two incoherent poles of the rotor Green's function. These poles persist into the bad metal regime across the Mott transition, as can be seen from the results for $U/U_c < 1$.

from above, the evolution of the rotor spectral function (integrated over \mathbf{k}) is illustrated by the results shown in Fig. (3) for $U/U_c = 1.25, 1.1$. The incoherent peaks are still well-defined, but the peak locations naturally shift towards smaller ω . Therefore J_{ex} increases as $U \rightarrow U_c^+$.

Moving into the bad-metal regime, where $U < U_c$, the coherent electron weight Z is non-zero but still small. Importantly, the incoherent peaks remain in the rotor spectral function, as illustrated by the results shown in Fig. (3) for $U/U_c = 0.9, 0.75, 0.5$. We still have well-defined exchange interaction, J_{ex} from integrating out the incoherent spectra. Importantly,

$$\begin{aligned} J_{\text{ex}} &= \int \frac{d\nu}{2\pi} G_{X,\text{inc}}(\nu; i, i) G_{X,\text{inc}}(\nu; j, j) \\ &= \sqrt{\frac{U}{U_c}} \int \frac{d\nu'}{2\pi} G_{X,c}(\nu'; i, i) G_{X,c}(\nu'; j, j) \\ &= J_{\text{ex}}(U_c)(1 - Z), \end{aligned} \quad (18)$$

where $G_{X,c}(\nu'; \mathbf{k}) = (\nu'^2/U_c + \lambda_c + Q_X \epsilon_{\mathbf{k}})^{-1}$ is transformed from $G_{X,\text{inc}}(\nu; \mathbf{k})$ by letting $\nu' = \nu\sqrt{U_c/U}$. Because the spectral weight in the incoherent part is lost to the coherent part, the exchange interaction will decrease as U decreases from U_c .

We therefore expect that J_{ex} will be maximized around U_c . This is indeed seen in the calculated result near the Mott transition, shown in Fig. (4).

The case of multiple orbitals : In iron pnictides, the atomic part includes the Hund's rule coupling. For simplicity, we

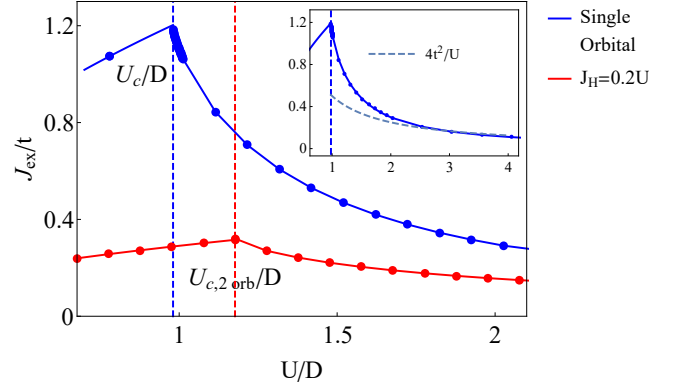


FIG. 4. (Color online) The calculated J_{ex} plotted as a function of U/t from the bad-metal regime to the insulating side for both the single orbital case (blue) and the simple two-orbital model (red). For both cases, the exchange interactions are seen to be maximized around the Mott transition. The inset shows J_{ex} for the single orbital case on the insulating side up to large values of U/t ; the axes are the same as in the main plot. The navy dashed line corresponds to the standard result for the large- U limit, $J_{\text{ex}} \simeq \gamma t^2/U$ with $\gamma = 4$.

consider the minimal two-orbital model[38]

$$\begin{aligned} H_{\text{at},2\text{orb}} &= \sum_i \left(U \sum_s n_{is\uparrow} n_{is\downarrow} + (U' - \frac{J_H}{2}) \sum_{\sigma,\sigma'} n_{i1\sigma} n_{i2\sigma'} \right. \\ &\quad \left. - 2J_H \mathbf{S}_{i1} \cdot \mathbf{S}_{i2} \right), \end{aligned} \quad (19)$$

where $U' = U - 2J_H$ denotes the intraorbital Coulomb repulsion[39].

In iron pnictides, J_H is a fraction of U , thus a relevant energy scale in the atomic limit. Therefore, we solve the atomic energy levels with the J_H term via exact diagonalization, and match the effect of Hund's rule coupling in the atomic within the above slave rotor framework.

At half-filling, the atomic ground state(s) are the spin-1 triplets states, with an charge excitation energy $E(N = 3) + E(N = 1) - 2E(N = 2)_{S=1} = U + J_H$. Near the half-filled insulating state, it is the superexchange interactions among the spin-1 local or quasi-local moments that are of interest. In Ref. [40], a renormalization of $U \rightarrow \tilde{U} = U + J_H$ is used to account for the correct Mott gap. However, the effect of Hund's coupling on spins is not accounted for, i.e. the formation of the spin-1 local moments. We further introduce a spinon Hund's coupling, which provides the correct spin-1 triplets when diagonalized in the atomic limit. Within the slave rotor construction, the spinon Hund's coupling does not affect the rotor spectrum. Hence, we account for the correct spin-1 moments, as well as the correct charge excitations. However, we must note that the contribution of Hund's coupling to the ground state energy is double-counted, and the Green's function is not as good. This is because the mapping only accounts for the first excited state in contrast to the $SU(2)$ symmetric case where the full spectrum is described by the rotor field.

Then the superexchange interaction J_{eff} is computed in the same way via the two orbital slave rotor model with the renormalized \tilde{U} , either between the spinons, or the spin-1 operators. We always find that J_{eff} peak at U_c , even though the value of U_c is modified due to J_H . Numerical results for fixed $J_H = 0.2U$ among spinons are plotted as functions of U in Fig. (4). These interactions are more complex, because the appropriate spinon bilinears may not only involve the spin degrees of freedom, but also the orbital ones. The form of the latter will depend on the filling factors. Here we will concentrate on the interactions that involve only the spins, in which case the effective interaction will be the on-site Hund's couplings and intersite exchange interactions of the following form [6]: $\sum_{ij,\tau,\tau'} J_{ij}^{\tau\tau'} \mathbf{S}_i^\tau \cdot \mathbf{S}_j^{\tau'}$, where τ, τ' label the orbitals. The exchange interaction forms a matrix in the orbital basis.

Discussions: We have used the slave rotor approach here as a means to capture the incoherent part of the electron spectral weight. An attractive alternative approach is a slave-spin method, either in the Z_2 form [41] or in the $U(1)$ form [42]. The $U(1)$ formulation, in particular, properly describes the Mott insulating phase and should therefore be able to capture the incoherent part of the electron spectral weight in a similar fashion. This approach could be advantageous to understanding the dependence of the exchange interactions on the Hund's coupling [21]. Nonetheless, our procedure presented here already provides the conceptual basis for deriving the exchange interactions in the bad-metal regime (in other words, not just on the insulating side).

Although beyond the saddle point, a strongly coupled gauge theory is found [37], the high energy part of the spectrum does *not* involve a strongly coupled gauge theory. Provided U/t is not too small (i.e., provided we stay in the bad-metal regime), the effect is not important. The calculation of the exchange interaction can be done with a low-energy cutoff in the integration over the slave-rotor spectral functions, and the result is insensitive to this cutoff.

Finally, we have focused on the bi-linear exchange interaction. Our procedure also contains processes for multi-spin exchange interactions. These include both the bi-quadratic couplings and ring-exchange interactions.

Implications for the Iron-based Superconductors: As already discussed in the introduction, all iron-based superconductors fall in the bad-metal regime. They are also inherently multi-orbital systems with a sizable ratio of the Hund's coupling to the Hubbard U , J_H/U . Through our analysis of the multi-orbital Hubbard model with a ratio of J_H/U comparable to that for the iron-based superconductors, our work sheds light on the exchange interactions in these systems.

We note that the exchange interaction we have derived operates between the physical spin degrees of freedom. Through Eq. (2) and Eq. (10), we see that the single-electron spectral weight contains a coherent part, with weight Z , and an incoherent part, with weight $1 - Z$. In the bad-metal regime, Z is small. Therefore, the physical spin degree of freedom is predominantly generated by the incoherent single-electron excitations with the remainder contribution coming from the

small coherent single-electron excitations near the Fermi energy [7, 43]. This is to be compared with the fully localized regime, where the coherent electron weight vanishes ($Z = 0$) and the spin degrees of freedom would be just local moments.

Finally, superconductivity can be driven by the short-range exchange interactions. Work by some of the co-authors here [44] have shown that the pairing amplitude increases with increasing J_{ex}/D^* , where D^* is the renormalized bandwidth. Since D^* decreases as the Mott transition is approached, and J_{ex} is maximized there, the superconducting pairing amplitude is expected to be the largest near the boundary of localization and delocalization.

To summarize, we have presented a microscopic approach to determine the exchange interactions in the bad metal regime where the single-electron excitation weight mostly lies in the incoherent part. From concrete calculations, we have demonstrated that the exchange interaction is the largest near the boundary of localization and delocalization. Correspondingly, superconductivity driven by short-range spin-exchange interactions is expected to have the largest pairing amplitude in such a regime.

This work was completed prior to the passing of one of the authors (E.A.). The other three authors (W.D., R.Y. and Q.S.) are grateful to have had the opportunity to collaborate with him. We would like to acknowledge the useful discussions with E. Bascones, S. A. Kivelson and other participants of the KITP program on "Magnetism, Bad Metals and Superconductivity: Iron Pnictides and Beyond". This work has been supported in part by the U.S. Department of Energy, Office of Science, Basic Energy Sciences, under Award No. DE-SC0018197 and the Robert A. Welch Foundation Grant No. C-1411 (W.D. and Q.S.). R.Y. was partially supported by the National Science Foundation of China Grant No. 11674392, and the Fundamental Research Funds for the Central Universities and the Research Funds of Renmin University of China. All of us acknowledge the support provided in part by the National Science Foundation under Grant No. NSF PHY-1748958 at KITP, UCSB. We also acknowledge the hospitality of the Aspen Center for Physics (NSF Grant No. PHY-1607611, Q.S. and E.A.).

APPENDIX: APPLICATION TO TWO-ORBITAL MODEL: ROLE OF HUND'S COUPLING

To account for Hund's rule coupling in various models that describe the iron pnictides, we follow Ref. [40] to map the Hund's rule coupling to renormalization of the repulsion $U \rightarrow \tilde{U}$.

The atomic (local) part of the minimal two orbital model reads

$$H_{\text{int}} = \sum_i \left(U \sum_s n_{is\uparrow} n_{is\downarrow} + (U' - J_H/2) n_{i1} n_{i2} - 2J_H \mathbf{S}_{i1} \cdot \mathbf{S}_{i2} \right). \quad (20)$$

We diagonalize H_{int} , and show several typical energies and eigenstates at different filling factors in Table I.

TABLE I. Typical eigenstates and the corresponding eigenenergies of H_{int} obtained by exact diagonalization. The eigenstates are labeled by the four occupation numbers $n_{i,\sigma}$ of orbital $i = 1, 2$ and spin σ .

$n_{1\uparrow}$	$n_{1\downarrow}$	$n_{2\uparrow}$	$n_{2\downarrow}$	E
1	0	0	0	0
...				
1	0	1	0	$U' - J_H$
1	0	0	1	$U' + J_H$
1	1	0	0	U
...				
1	1	1	0	$2(U' - J_H/2) + U$
...				
1	1	1	1	$2(U + 2U' - J_H)$

Our focus is superexchange interaction of the $\langle \hat{N}_i \rangle = 2$ states. It is easy to verify that the energy spacing for the relevant excitations is $\Delta E = (E_i(N = 1) - E_i(N = 2)) + (E_i(N = 3) - E_i(N = 2)) = U + J_H$ for the $S = 1$ triplet states. For the $S = 0$ singlet state, this energy spacing is $\Delta E = U - 3J_H$. Near the Mott insulating phase, the $S = 1$ triplets are the ground state. Even though the low lying $S = 0$ state has lower excitation energy, it cannot participate in the superexchange virtual process. To further account for the spin splitting, we also include a spinon Hund's coupling

$$H_{f,J_H} = -2J_H \sum_i \mathbf{S}_{f,i1} \cdot \mathbf{S}_{f,i2}, \quad (21)$$

where $\mathbf{S}_{f,i\sigma} = \sum_{\alpha\beta} \frac{1}{2} f_{i\sigma\alpha}^\dagger \boldsymbol{\sigma}_{\alpha\beta} f_{i\sigma\beta}$.

Therefore, we can account for both the charge excitation energy as well as the spin splitting of the two orbital Hubbard with Hund's coupling via

$$\tilde{H}_{at} = \sum_{i,\alpha} f_{i\alpha}^\dagger (\partial_\tau + h_i) f_{i\alpha} + \sum_i (\tilde{U} \hat{L}_i^2 / 2 + h_i \hat{L}_i) + H_{f,J_H}, \quad (22)$$

with $\tilde{U} = U + J_H$. Since H_{f,J_H} preserves the spinon number, $h_i = 0$ still holds at half filling.

* wenxinding@gmail.com

† deceased

- [1] Y. Kamihara, T. Watanabe, M. Hirano, and H. Hosono, *J. Am. Chem. Soc.* **130**, 3296 (2008).
 [2] C. de la Cruz, Q. Huang, J. W. Lynn, J. Li, W. Ratcliff, J. L. Zarestky, H. a. Mook, G. F. Chen, J. L. Luo, N. L. Wang, and P. Dai, *Nature* **453**, 899 (2008).
 [3] E. Abrahams and Q. Si, *J. Phys. Condens. Matter* **23**, 223201 (2011).

- [4] N. E. Hussey, K. Takenaka, and H. Takagi, *Philoso. Mag.* **84**, 2847 (2004).
 [5] M. M. Qazilbash, J. J. Hamlin, R. E. Baumbach, L. Zhang, D. J. Singh, M. B. Maple, and D. N. Basov, *Nat. Phys.* **5**, 647 (2009).
 [6] Q. Si and E. Abrahams, *Phys. Rev. Lett.* **101**, 076401 (2008).
 [7] Q. Si, E. Abrahams, J. Dai, and J.-X. Zhu, *New J. Phys.* **11**, 045001 (2009).
 [8] K. Haule, J. H. Shim, and G. Kotliar, *Phys. Rev. Lett.* **100**, 226402 (2008).
 [9] M.-H. Fang, H.-D. Wang, C.-H. Dong, Z.-J. Li, C.-M. Feng, J. Chen, and H. Q. Yuan, *Europhys. Lett.* **94**, 27009 (2011).
 [10] P. Gao, R. Yu, L. Sun, H. Wang, Z. Wang, Q. Wu, M. Fang, G. Chen, J. Guo, C. Zhang, D. Gu, H. Tian, J. Li, J. Liu, Y. Li, X. Li, S. Jiang, K. Yang, A. Li, Q. Si, and Z. Zhao, *Phys. Rev. B* **89**, 094514 (2014).
 [11] R. Yu, J.-X. Zhu, and Q. Si, *Phys. Rev. Lett.* **106**, 186401 (2011).
 [12] E. Dagotto, *Rev. Mod. Phys.* **85**, 849 (2013).
 [13] J.-X. Zhu, R. Yu, H. Wang, L. L. Zhao, M. D. Jones, J. Dai, E. Abrahams, E. Morosan, M. Fang, and Q. Si, *Phys. Rev. Lett.* **104**, 216405 (2010).
 [14] M. Yi, D.H. Lu, R. Yu, S. C. Riggs, J.-H. Chu, B. Lv, Z. Liu, M. Lu, Y.-T. Cui, M. Hashimoto, S.-K. Mo, Z. Hussain, C. Chu, I. Fisher, Q. Si, and Z.-X. Shen, *Phys. Rev. Lett.* **110**, 067003 (2013).
 [15] R. Yu and Q. Si, *Phys. Rev. Lett.* **110**, 146402 (2013).
 [16] C. Fang, H. Yao, W.-F. Tsai, J. Hu, and S. A. Kivelson, *Phys. Rev. B* **77**, 224509 (2008).
 [17] C. Xu, M. Müller, and S. Sachdev, *Phys. Rev. B* **78**, 020501(R) (2008).
 [18] T. Yildirim, *Phys. Rev. Lett.* **101**, 057010 (2008).
 [19] F. Ma, Z.-Y. Lu, and T. Xiang, *Phys. Rev. B* **78**, 224517 (2008).
 [20] M. Han, Q. Yin, W. Pickett, and S. Savrasov, *Phys. Rev. Lett.* **102**, 107003 (2009).
 [21] M. J. Calderon, G. Leon, B. Valenzuela, and E. Bascones, *Phys. Rev. B* **86**, 104514 (2012).
 [22] K. Seo, B. A. Bernevig, and J. Hu, *Phys. Rev. Lett.* **101**, 206404 (2008).
 [23] W.-Q. Chen, K.-Y. Yang, Y. Zhou, and F.-C. Zhang, *Phys. Rev. Lett.* **102**, 047006 (2009).
 [24] A. Moreo, M. Daghofer, J. Riera, and E. Dagotto, *Phys. Rev. B* **79**, 134502 (2009).
 [25] W. Lv, F. Krüger, and P. Phillips, *Phys. Rev. B* **82**, 045125 (2010).
 [26] G. Uhrig, M. Holt, J. Oitmaa, O. Sushkov, and R. Singh, *Phys. Rev. B* **79**, 092416 (2009).
 [27] H. Ishida and A. Liebsch, *Phys. Rev. B* **81**, 054513 (2010).
 [28] G. Giovannetti, C. Ortix, M. Marsman, M. Capone, J. van den Brink, and J. Lorenzana, *Nat. Commun.* **2**, 398 (2011).
 [29] E. Bascones, B. Valenzuela, and M. J. Calderón, *Phys. Rev. B* **86**, 174508 (2012).
 [30] M. Wang, C. Fang, D.-X. Yao, G. Tan, L. W. Harriger, Y. Song, T. Netherton, C. Zhang, M. Wang, M. B. Stone, W. Tian, J. Hu, and P. Dai, *Nat. Commun.* **2**, 580 (2011).
 [31] W. Bao, Q.-Z. Huang, G.-F. Chen, D.-M. Wang, J.-B. He, and Y.-M. Qiu, *Chin. Phys. Lett.* **28**, 086104 (2011).
 [32] J. Zhao, H. Cao, E. Bourret-Courchesne, D.-H. Lee, and R. J. Birgeneau, *Phys. Rev. Lett.* **109**, 267003 (2012).
 [33] D. G. Free and J. S. O. Evans, *Phys. Rev. B* **81**, 214433 (2010).
 [34] E. E. McCabe, C. Stock, E. E. Rodriguez, a. S. Wills, J. W. Taylor, and J. S. O. Evans, *Phys. Rev. B* **89**, 100402 (2014).
 [35] S. Florens and A. Georges, *Phys. Rev. B* **66**, 165111 (2002).
 [36] S. Florens and A. Georges, *Phys. Rev. B* **70**, 035114 (2004).
 [37] S.-S. Lee and P. A. Lee, *Phys. Rev. Lett.* **95**, 036403 (2005).

- [38] S. Raghu, X. L. Qi, C. X. Liu, D. J. Scalapino, and S. C. Zhang, [Phys. Rev. B **77**, 220503\(R\) \(2008\)](#).
- [39] C. Castellani, C. R. Natoli, J. Ranninger [Phys. Rev. B **18**, 4945 \(1978\)](#).
- [40] O. N. Meetei, O. Erten, M. Randeria, N. Trivedi, and P. Woodward, [Phys. Rev. Lett. **110**, 087203 \(2013\)](#).
- [41] L. de' Medici, A. Georges, and S. Biermann, [Phys. Rev. B **72**, 205124 \(2005\)](#).
- [42] R. Yu and Q. Si, [Phys. Rev. B **86**, 085104 \(2012\)](#).
- [43] J.H. Dai, Q.S. Si, J.-X. Zhu, and E. Abrahams, PNAS **106**, 4118 (2009).
- [44] R. Yu, P. Goswami, Q. Si, P. Nikolic, and J.-X. Zhu, [Nat. Commun. **4**, 2783 \(2013\)](#).